Acceleration Mechanism of Growth Rates under Shear Flow Due to the Oriented Melt−The Novel Morphology of Spiral Crystal (Spiralite)−

Kaori Watanabe,*,† Kiyoka Okada,† Akihiko Toda,† Shinichi Yamazaki,† Takashi Taniguchi,‡ Kiyohito Koyama,‡ Koji Yamada,§ and Masamichi Hikosaka†

Soft material physics group, Faculty of Integrated Arts and Sciences, Hiroshima University, 1-7-1 Kagamiyama, Higasshi Hiroshima 739-8521, Japan, Department of Polymer Science and Engineering, Yamagata University, 4-3-16, Yonezawa 992-8510, Japan, and Kawasaki Development Center, R&D Department, SunAllomer Ltd. 3-2 Yako 2-chome, Kawasaki-ku, Kawasaki, 210-8548, Japan

Received April 19, 2005; Revised Manuscript Received December 1, 2005

ABSTRACT: Isothermal crystallization of three-dimensional (3D) spherulites from the bulky melt under low shear rate flow was studied based on new in situ observation along a direction perpendicular to the flow velocity gradient plane (*XZ* plane) by means of optical microscope, where *X*- and *Z*-axes are perpendicular and parallel to the flow direction, respectively. Spherulites are rotating. A novel "spiral pattern" was found on the surface of the rotating "half-spherulite" near the surface of the melt for the first time. The half-spherulite is named "spiralite" which enabled us to have a visible image of the rotation of spherulite. Hence, we could detect the growth rate around the *Z*-axis $V(Z)$ and that around the *X*-axis $V(X)$ by using the spiral pattern. We could experimentally obtain $V(Z) > V(X)$ in this study. From kinetic viewpoint, this fact indicates that free energy for formation of a critical nucleus around the *Z*-axis is smaller than that around the *X*-axis. From this, it is concluded that the "oriented melt" is formed around the *Z*-axis. We proved it theoretically by showing that micro shear rate $\dot{\gamma}(Z)$ on the interface around the *Z*-axis significantly increases and chains will be elongated even when macro $\dot{\gamma}$ is low ($\dot{\gamma} < 10\ s^{-1}$). With increase of $\dot{\gamma}(Z)$, the chain elongation will overcome the entropic relaxation, that results in formation of the "oriented melt". Crystallization mechanism under low shear flow is proposed that the growth rate of spherulite or shish is accelerated around interface, due to formation of the "oriented melt". Finally, we proposed a possible relationship between melt structure and crystallization under anisotropic and isotropic external fields.

1. Introduction

In the case of the polymer system, it is logical that isotropic and anisotropic external fields, such as quiescent condition and elongational or shear flow, respectively, significantly affect the melt structure and that the melt structure does the crystallization behavior. When the melt of polymers is put in the isotropic quiescent field, the "isotropic melt" is formed where molecular conformation of chains becomes random coil. Although the effect of anisotropic external field on the crystallization mechanism is interesting and important in polymer science and processing, it has not been well solved. In this paper, we will solve the unsolved problem.

1.1. Effects of External Fields on the Melt Structures and Crystallization. (a) High Strain Rate. When a strong anisotropic elongational or shear field is applied to the melt, it is expected that the chains are elongated and the "oriented melt" is formed due to high strain rate.

Kotaka et al.[1,2] measured simultaneously the tensile stress and birefringence (Δn) of the melt of polymers under elongational flow (strain rate $\dot{\epsilon} = 0.005-1.0\ s^{-1}$). They showed that Δn of polystyrene (PS) and low-density polyethylene (LDPE) increased up to $\Delta n \cong 10^{-2}$ and 10^{-3}, respectively. They concluded that the above results show formation of the "segmental orientation" that should correspond to the "uniform oriented melt".

In the case of high $\dot{\gamma}$ ($\dot{\gamma} > 10^2 s^{-1}$), Fritzsche et al.[3] observed time evolution of crystallinity and the induction time (τ) for the appearance of crystallinity of poly(ethylene oxide) (PEO) under high shear flow (maximum $\dot{\gamma}$ is 168 s^{-1}) by using a concentric cylinder dilatometer. They showed that τ under shear flow was shorter than that in the quiescent state and they speculated that the nucleation and lateral growth rates (*I* and *V*) were accelerated within the "oriented melt" due to chain elongation.

(b) Low Strain Rate. Many researchers[4−10] have studied the melt crystallization under low $\dot{\gamma}$ ($\dot{\gamma} < 10\ s^{-1}$), using various instruments, such as parallel-plate type[4] and rotating ones[5−8] and showed coexistence of spherulites and interesting morphologies of "shish"[7−10] and "row-nucleation"[4,6] by means of optical microscope. The latter should correspond to the "oriented melt". Wolkowicz et al.[5] showed that nucleation rate (*I*) of spherulites of polybutene-1 (PB-1) was greatly accelerated but that growth rate (*V*) of that was slightly accelerated. They speculated that the acceleration of *I* is due to "chain alignment within the melt by increasing number of nuclei which act as filler particles and increase stress in the system". Their speculation assumed formation of the uniform oriented melt. Monasse et al.[4] showed that *I* and *V* of spherulites in row-nucleation of polyethylene (PE) were accelerated and growth was anisotropy. They assumed that acceleration of *V* is due to "increase of equilibrium melting temperature T_m^0 emanating from an entropy loss due to the chain orientation". They speculated that "the anisotropy of growth can be discussed as an effect of chain orientation with respect to the growth front of lamellae and of a local flow different from macroscopic shear flow". Their speculation means the

* To whom correspondence should be addressed. Telephone: +81-82-424-6538. Fax: +81-82-424-0757. E-mail: watanabe@vbl.hiroshima-u.ac.jp.
† Hiroshima University.
‡ Yamagata University.
§ SunAllomer Ltd.

10.1021/ma050825z CCC: $33.50
Published on Web 01/20/2006

formation of a locally oriented melt. Therefore, the mechanism of formation of the oriented melt and that of acceleration of I and V under low strain rate are important unsolved problems.

Alfonso et al.[11] studied crystallization of PB-1 under shear flow by using a fiber pull-out instrument. According to the thermomechanical model proposed by Monasse,[12] $\dot{\gamma}$ were estimated to be order of several hundreds of reciprocal seconds at the fiber−melt interface. They observed "cylindrical morphology" around the trace of the pulled fiber. The "cylindrical morphology" is similar to the row-nucleation. They considered that the cylindrical morphology is due to the formation of the orientation of segments that corresponds to the oriented melt. In this case, $\dot{\gamma}$ should be instantaneously high during the pulling process, and then $\dot{\gamma}$ should become zero.

1.2. Kinetic Relationship between the Melt Structure and Crystallization. According to classical nucleation theory,[13] the lateral growth rate (V) is given by

$$V = V_0 \exp\left(\frac{-\Delta G^*}{mkT}\right) = V_0 \exp\left(\frac{-B}{m\Delta T}\right) \quad (1)$$

where V_0, ΔG^*, m, k, T, B, and ΔT are prefactor, free energy of necessary for formation of a critical secondary nucleus, a constant ($m = 1$ for single and $m = 2$ or 3 for multinucleation), Boltzmann constant, temperature, a constant that is proportional to ΔG^*, and degree of supercooling, respectively. ΔG^* and B are given by

$$\Delta G^* \propto B \propto \sigma_e \sigma \quad (2)$$

where σ_e and σ are the end and side surface free energies, respectively. ΔT is defined by

$$\Delta T \equiv T_m^{\,0} - T_c \quad (3)$$

where T_m^0 is the equilibrium melting temperature and T_c is the crystallization temperature. Hereafter the lateral growth rate will be simply named the growth rate.

As the $\sigma_e\sigma$ and ΔG^* within the oriented melt should be smaller than those within the isotropic melt for the same ΔT, V within the oriented melt should be larger than that within the isotropic melt.

1.3. Formation of Shish within the Oriented Melt on the Interface under Low Shear Rate. We observed a nucleation and growth of shish under low shear rate ($\dot{\gamma} = \sim 0.5-5\ s^{-1}$).[7,8] ΔT dependence of the lateral growth rate of shish perpendicular to the flow direction (V_{shish}) was fitted by eq 1, that indicates that V_{shish} is mainly controlled by the secondary critical nucleation process. The B of shish (B_{shish}) was much smaller than that of spherulite under quiescent condition, that suggests formation of the oriented melt on the side surface of shish. From similar observation and kinetic analysis of nucleation of shish, a bundle nucleus from the oriented melt on the interface was proposed.

However, we proposed only a speculative model for the formation mechanism of the oriented melt on the interface. We proposed "on the side surface of shish, an adsorbed random coil is elongated by the shear flow and the oriented melt is formed. The origin of this elongation is that the entangled chains are moved by the shear flow." However this speculation is insufficient. Chain on the level with radius of gyration is not elongated, which will be shown in section 4.2. Therefore, we have to solve the formation mechanism of the oriented melt.

1.4. Crystallization in Injection Molding Processing. In injection molding processing, it is well-known that skin and core layers are formed around the surface and the center, respectively.[14] Shish, kebab, row-nucleation, or transcrystal are mainly formed in the skin, while spherulites are formed in the core. As formation of the skin and core significantly affects the physical properties of products, the formation mechanism of the skin and core is important. However, the mechanism has not been well solved. Therefore, we have to solve the mechanism.

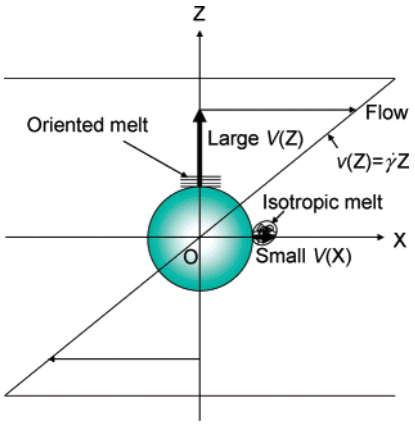

Figure 1. Schematic relationship between growth of a 3D spherulite and the melt structure under shear flow.

1.5. Purpose of This Study. The purpose of this study is to show an acceleration mechanism of growth rate of spherulites by presenting a formation mechanism of the "oriented melt" on the interface even when shear rate is low.

Figure 1 shows schematic projection of three-dimensional (3D) spherulite in the bulky melt under shear flow from a direction perpendicular to the flow velocity gradient plane. Within a short time, we can neglect the rotation of spherulite. Here we took an origin of $X-Z$ coordinate at the center of the spherulite. Horizontal and vertical axes (X and Z) are parallel and perpendicular to the shear direction, respectively. If we will be able to show experimentally that normal lateral growth rate at the interface around the Z-axis $V(Z)$ is larger than that around the X-axis $V(X)$, it will be confirmed that the oriented melt is formed around the Z-axis and the isotropic melt is formed around the X-axis from the discussion in section 1.2. Here $V(Z)$ and $V(X)$ are normal lateral growth rates of radial lamellae along Z- and X-axes, respectively. On the basis of the above experimental confirmation, it will be theoretically shown that the $\dot{\gamma}$ increases significantly on the interface around the Z-axis, while it does not around the X-axis. A possible relationship between the melt structure and crystallization under anisotropic and isotropic external fields will be proposed.

2. Experimental Section

2.1. Samples. PB-1 ($M_w = 18 \times 10^4$, $M_w/M_n = 3.3$) and isotactic polypropylene (iPP) (K1014, supplied by Chisso Petrochemical Corp., Ltd., $M_w = 22 \times 10^4$, $M_w/M_n = 2.9$) were used, where M_w and M_n are weight- and number-averaged molecular weights, respectively.

2.2. Instruments. To confirm the above speculation, we developed a new coaxial cylinder type instrument (Figure 2).[15] We named it a shear flow observation apparatus (SFO). The gap between inner and outer cylinders is 0.5 mm. The shape of the sample is a "doughnut ring". It is important that the top surface of the doughnut ring has its free surface facing the air to avoid any friction. The inner cylinder is rotated to apply shear flow to the sample, and the outer cylinder is fixed. Hence we will name them rotating and fixed cylinders, respectively. It enables direct observation of growth rates of crystals along a direction perpendicular to the flow velocity gradient plane (XZ plane) by means of optical

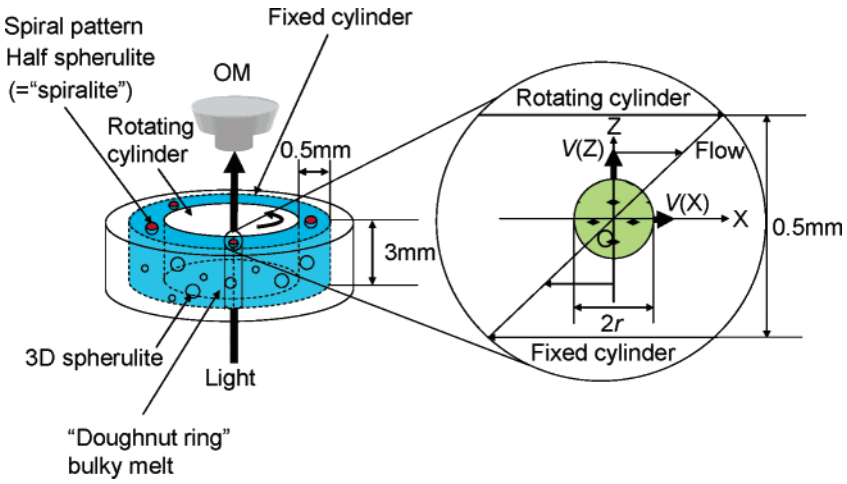

Figure 2. Schematic illustration of a shear flow observation apparatus (SFO) and growth of spherulites in the bulky melt under shear flow. 3D spherulites are formed within the bulky melt and "half-spherulites (="spiralite", as explained in section 3.1)" are formed near the free surface of the melt.

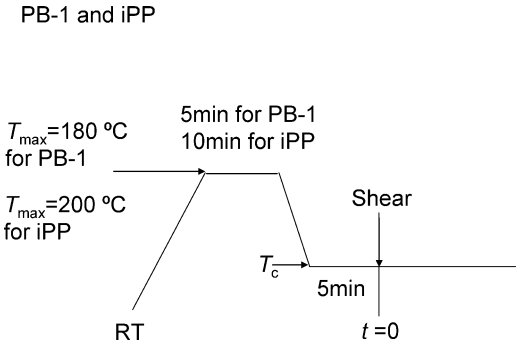

Figure 3. Crystallization process of PB-1 and iPP showing crystallization parameters.

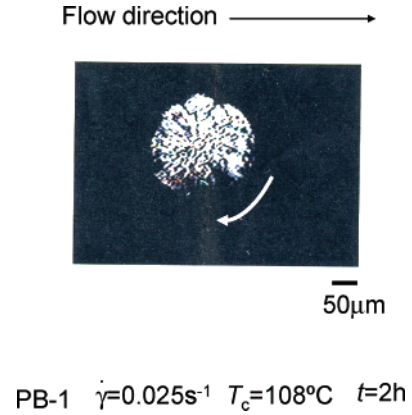

Figure 4. Typical polarizing optical micrograph of a rotating 3D spherulite of PB-1 under shear flow ($\dot{\gamma}$ = 0.025 s^{-1}, T_c = 108 °C).

microscopy, which has been impossible for the previous instruments, such as parallel-plate type and fiber pull-out ones.[15] As the new SFO enables us to observe directly the effect of shear flow on crystallization, it becomes possible to make clear the formation mechanism of a spherulite, shish or row-nucleated structure under shear flow. Therefore, the SFO has a significant advantage in the study of crystallization under shear flow. The crystallization behavior was observed by means of polarizing optical microscope (Leica Company, DMR HC) and was recorded by using a CCD video camera system (Simazu Co., Ltd. CCD-SII). Thermocouples were inserted into the sample and connected to a temperature controller.

2.3. Crystallization and Morphology. PB-1 and iPP were once melted at 180 °C for 5 min and 200 °C for 10 min, respectively, and crystallized in the following ranges range of T_c: 102−108 °C for PB-1 and 138−145 °C for iPP (Figure 3). After the crystals were kept for 5 min at T_c, shear was added. The range of $\dot{\gamma}$ was 0.01−0.1 s^{-1}. In our experimental condition, before applying shear (after 5 min of crystallization) spherulites were generated when T_c was rather low, but they were not generated when T_c was rather high. It is not important to distinguish whether spherulites were generated before or after applying shear, because the observation of growth was carried out on large spherulites. Crystallization time t was counted after adding shear in the case of shear flow and after quenching to T_c under quiescent conditions.

In this study, we will show formation of 3D spherulite in the "doughnut ring" like bulky melt. When a spherulite grows near the free surface of the melt, "half-spherulite" is formed. In situ observation of growing 3D or half-spherulites by means of optical microscope is schematically illustrated in Figure 2. The half-spherulite was quenched, and the detailed morphology of the top surface was observed by means of laser microscopy (KEYENCE, VK-9500). To obtain three-dimensional information on structure, the quenched half-spherulites were sliced along *XY*-plane every 20 μm using a microtome and observed by means of optical microscope.

3. Results

3.1. Novel Morphology of "Spiralite". Many 3D spherulites were generated in the "doughnut ring" like bulky melt as schematically illustrated in Figure 2. Figure 4 shows a typical in situ polarizing optical micrograph of the growing 3D spherulite of PB-1 ($\dot{\gamma}$ = 0.025 s^{-1} T_c = 108 °C). They were rotating slowly, but it was impossible to observe correctly the rotating behavior, as the 3D spherulite showed uniform dot pattern (Figure 4).

When a nucleus is generated near the free surface of the melt (Figure 2), a "half-spherulite" is formed. The half-spherulite showed the novel morphology of "spiral pattern" on the top surface as high as the free surface of the melt (Figure 5). The spiral pattern was double one. Hence we named the half-spherulite "spiralite". It is interesting that the spiral pattern clearly showed the rotating behavior of the half-spherulite-(="spiralite") (Figure 5a). Parts a and b of Figure 5 show typical in situ polarizing optical micrographs of the spiral pattern of growing half-spherulites (="spiralite") of PB-1 ($\dot{\gamma}$ = 0.1 s^{-1} T_c = 102 °C) and iPP ($\dot{\gamma}$ = 0.1 s^{-1} T_c = 138 °C), respectively. Therefore, formation of the spiral pattern should be seen for any material.

Parts a−c of Figure 6 show morphology of half-spherulites (="spiralite") of PB-1, crystallized under the same condition

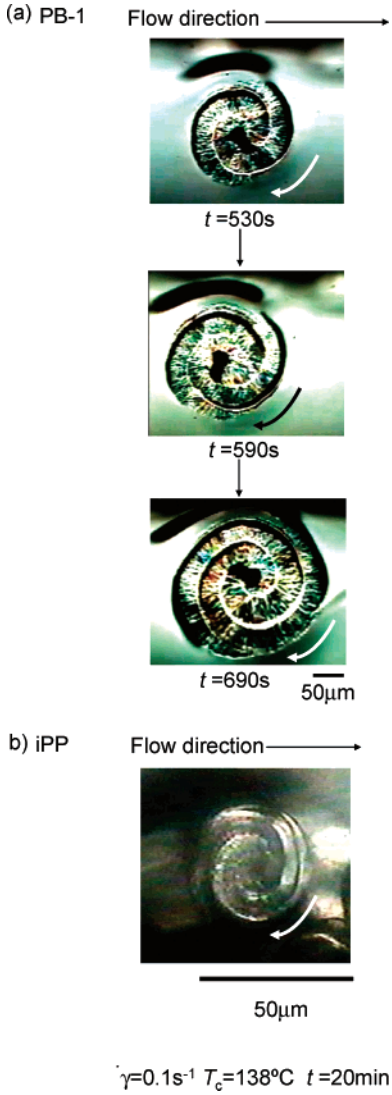

Figure 5. Typical in situ polarizing optical micrographs of rotating spiral pattern of growing half-spherulites (="spiralite") of (a) PB-1 ($\dot{\gamma}$ = 0.1 s^{-1}, T_c = 102 °C) and (b) iPP ($\dot{\gamma}$ = 0.1 s^{-1}, T_c = 138 °C). t indicates time after applying shear.

($\dot{\gamma}$ = 0.1 s^{-1}, T_c = 102 °C). Figure 6a shows in situ optical micrograph of a top view of the spiral pattern of the growing half-spherulite (="spiralite"). Dotted circle indicates the outline of the spherulite. Double spiral solid curves indicating "double Archmedes spirals" (that we will show in section 3.8) were superimposed on the usual radial lamellar pattern that is well-known in two-dimensional (2D) spherulite. Radius of the circle is denoted as r. The averaged pitch of the double spiral (P) was 36 μm. Figure 6b shows a typical polarizing optical micrograph of central cross section of the half-spherulite (="spiralite") which was sliced along XY-plane. The dotted circle indicates outline of the spherulite at quenching. The radial pattern outside of the outline corresponds to the growth during quenching. On the top surface, periodic oscillation was observed. The pitch of the oscillation (P) was 36 μm which corresponds to that of the double spiral shown in Figure 6a. The bottom part of the half-spherulite (="spiralite") showed the same radial lamellar pattern that is well-known in the usual 2D spherulite formed under quiescent conditions. Figure 6c shows a typical laser microscope image of the surface of the same half-spherulite (="spiralite") as is shown in Figure 6b. The dotted circle corresponds to the outline of the spherulite. The micrograph clearly shows the steric double spiral pattern on the top surface

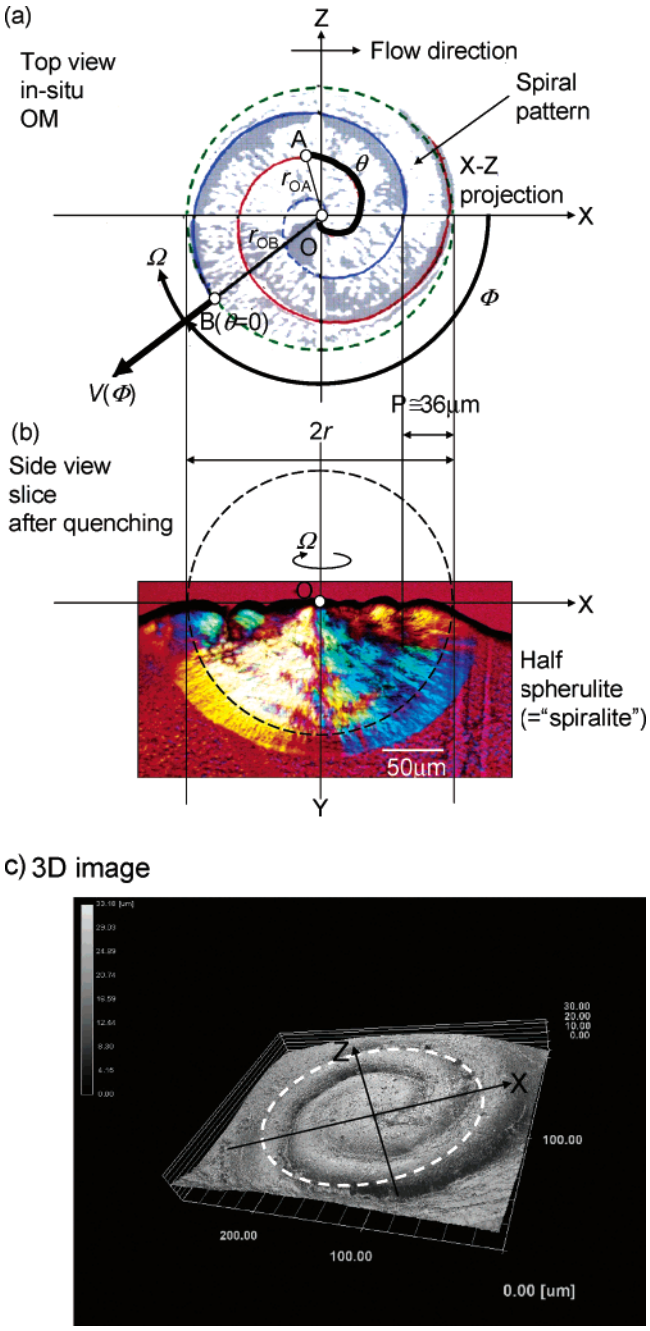

Figure 6. Three-dimensional morphology of "half-spherulite (="spiralite")" with spiral pattern of PB-1 crystallized at $\dot{\gamma}$ = 0.1 s^{-1} and T_c = 102 °C. (a) In situ optical micrograph of a top view of the spiral pattern of the growing "spiralite" (t = 600s). Double Archmedes spirals are superimposed by solid curves. (b) Polarizing optical micrograph of central cross section of the quenched half-spherulite "spiralite". (c) Laser microscope image of spiral pattern of the quenched half-spherulite "spiralite".

of the spherulite. The spiral patterns do not depend on material, $\dot{\gamma}$ and T_c. Therefore, we will focus to the typical spherulite of PB-1 crystallized under conditions of $\dot{\gamma}$ = 0.1 s^{-1} and T_c = 102 °C.

3.2. How to Detect *V*(Z) and *V*(X)? As spherulites are rotating, we have to observe normal lateral growth rate (V) at a fixed point on the growth front of a radial lamella in order to distinguish $V(Z)$ and $V(X)$, respectively. As it is impossible to observe quantitatively the rotating behavior of the 3D spherulite within the bulky melt, we observed it on the half-spherulite (="spiralite") by detecting the rotation of the spiral pattern. Therefore, the spiral pattern is important for visible image of

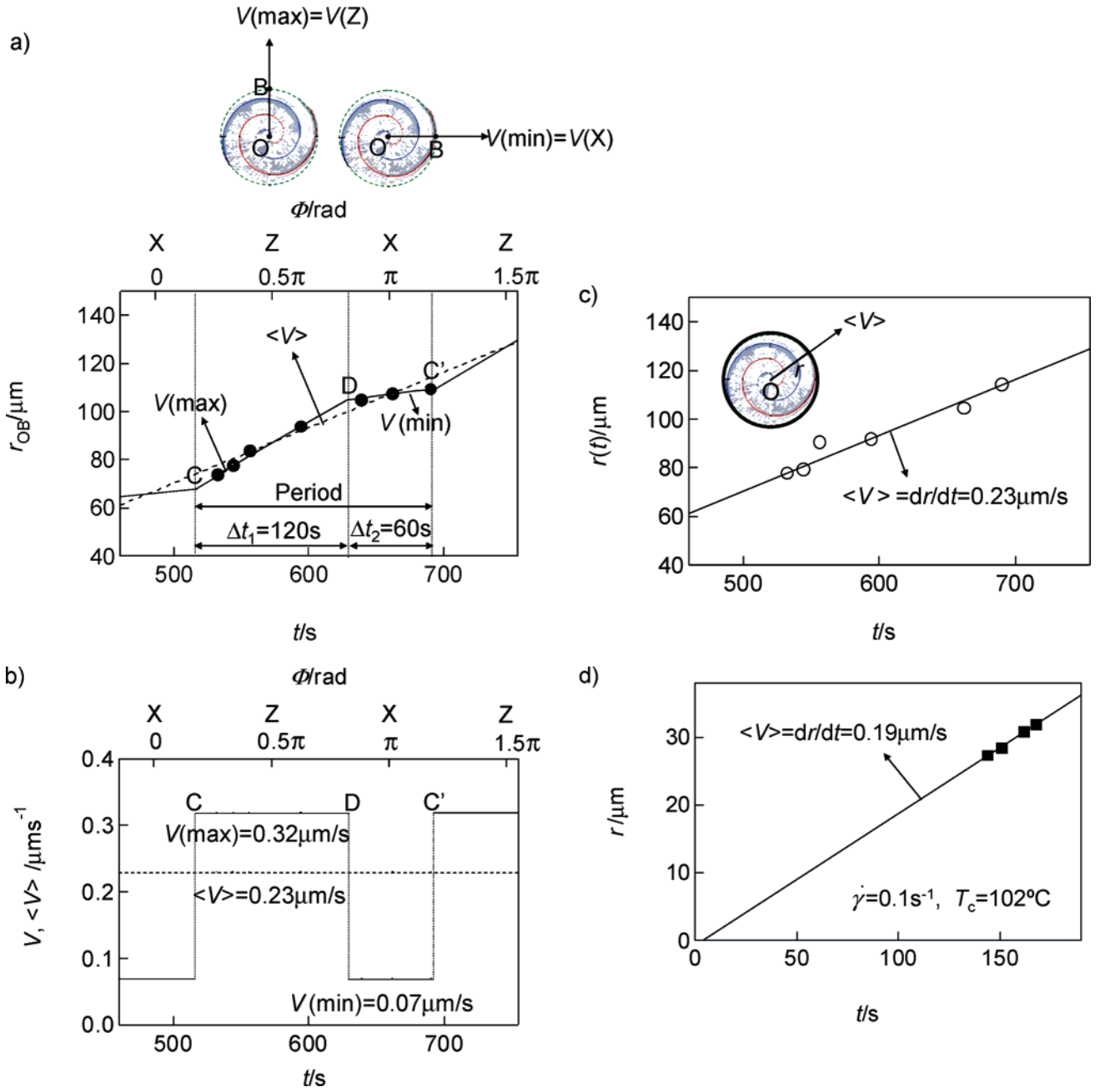

Figure 7. Growth of a half-spherulite (="spiralite") of PB-1 crystallized at $\dot{\gamma} = 0.1\ s^{-1}$ and $T_c = 102$ °C. (a) Plots of r_{OB} against t. Upper horizontal axis indicates Φ. The slope around the Z-axis was much larger than that around the X-axis. (b) Plots of V and $\langle V \rangle$ against t and Φ. V showed V(max) and V(min) periodically around the Z- and X-axes, respectively. (c) Plots of $r(t)$ against t. (d) Plots of r of the 3D spherulite of PB-1 against t crystallized under the same condition as in parts a−c.

rotation of spherulites. Thus, we could obtain $V(Z)$ and $V(X)$ of spherulites. The V of the rotating spherulite is obtained by

$$V = V(\Phi) = \frac{dr_{OB}}{dt} \tag{4}$$

where r_{OB} is the radius between the origin O of the spherulite and a fixed point B on the growth front of a radial lamella and Φ is the rotating angle between r_{OB} and X-axis (Figure 6a).

In the case of a 3D spherulite, we can only measure averaged growth rate ($\langle V \rangle$). It is also important that the V of radial lamella of the half-spherulite (="spiralite") should be the same as that of 3D spherulite. This will be confirmed by eq 9 in section 3.4; i.e., the averaged growth rate of the half-spherulite (="spiralite") ($\langle V \rangle$) and that of the 3D spherulite are equal. This is the same situation as is widely accepted in observation of V of spherulite in quiescent condition: V of 2D spherulite (=disk) should be the same as that of 3D spherulite.

3.3. Anisotropic Growth Rates of Rotating "Spiralite", *V*(Z) and *V*(X). Figure 5a shows that the size (r_{OB}) of the half-spherulite (="spiralite") increased with increase of t and that the spiral pattern rotated clockwise.

$r_{OB}(t)$ was plotted in Figure 7(a) as a function of t. Upper horizontal axis indicates Φ. $r_{OB}(t)$ increased linearly with increase of t or Φ. $r_{OB}(t)$ showed breakings at $\Phi \cong 0.8\pi$(point D) and 1.2π (point C′). The slope around the Z-axis ($\Phi = 0.5\pi$) was much larger than that around the X-axis ($\Phi = \pi$). The breaking in $r_{OB}(t)$ should be seen periodically from symmetry of the considering system. Thus, breakings are expected at C, D and C′ in Figure 7a. CC′ indicates a period. As large and small slopes are observed around the Z- and X-axes, respectively,

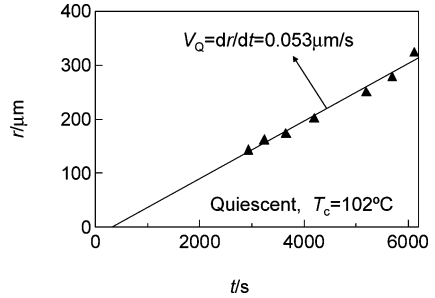

Figure 8. Plots of r of the spherulite of PB-1 against t in the quiescent state (T_c = 102 °C).

large and small V (denoted V(max) and V(min)) were obtained (Figure 7b), i.e.

$$V = V(\text{max}) = 0.32\ \mu\text{m/s} \quad \text{around } Z\text{-axis}$$
$$= V(\text{min}) = 0.07\mu\text{m/s} \quad \text{around } X\text{-axis} \tag{5}$$

V(max) was about 5 times as large as V(min). We will show in section 3.6 that V(max) and V(min) correspond to growth rates from the oriented and isotropic melt, respectively.

3.4. Averaged Growth Rate $\langle V\rangle$ of the Rotating "Spiralite". The radius of the outline of a spiralite $r(t)$ shown in Figure 6a and (b) are plotted against t in Figure 7c. $r(t)$ increased linearly with increase of t. Therefore, averaged growth rate of the spherulite ($\langle V\rangle$) was obtained by

$$\langle V\rangle \equiv \frac{dr}{dt} = 0.23\mu\text{m/s} \tag{6}$$

The $\langle V\rangle$ should also be given by the average of $V(\Phi)$, i.e.

$$\langle V\rangle \equiv \frac{1}{\Delta t_1 + \Delta t_2}\left(V(\text{max})\Delta t_1 + V(\text{min})\Delta t_2\right) = 0.23\ \mu\text{m/s} \tag{7}$$

where Δt_1 and Δt_2 indicate time interval between CD and DC′ in Figure 7a.

$\langle V\rangle$ of 3D rotating spherulite within the melt

$$\langle V\rangle = 0.19\ \mu\text{m/s} \tag{8}$$

was obtained (Figure 7d). Thus, we have

$$\langle V\rangle \text{ (half spherulite (="spiralite")) } \cong \langle V\rangle \text{ (3D spherulite)} \tag{9}$$

Therefore, it is confirmed that it is not necessary to distinguish $\langle V\rangle$ of the half-spherulite (="spiralite") and that of the 3D ones.

3.5. Growth Rate of a Spherulite in the Quiescent State. Figure 8 shows the plots of radius of a spherulite of PB-1 (r) against t in quiescent state (T_c = 102 °C) from which growth rate (denoted by V_Q)

$$V_Q = 0.053\ \mu\text{m/s} \tag{10}$$

was obtained. Therefore, we have

$$\langle V\rangle > V_Q \tag{11}$$

and

$$V_Q \cong V(\text{min}) \tag{12}$$

It is concluded that $\langle V\rangle$ and was accelerated as compared with V_Q for the same T_c. Equations 11 and 12 should be evidences of formation of the oriented and isotropic melts, respectively.

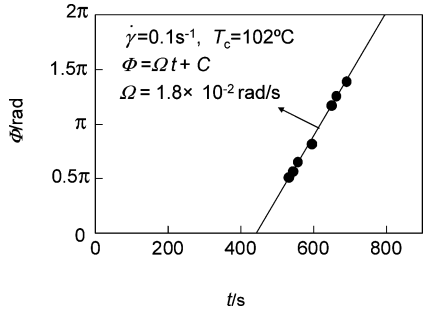

Figure 9. Plots of Φ of the half-spherulite (="spiralite") of PB-1 against t ($\dot{\gamma}$ = 0.1 s^{-1}, T_c = 102 °C). Ω was constant.

3.6. Evidence of the Oriented and Isotropic Melt. We will show here that V(max) and V(min) correspond to growth rates in the oriented and isotropic melt, respectively. Equations 5, 10, and 12 give a conclusion

$$V(\text{max}) = \frac{1}{4.5}V(\text{min}) > V(\text{min}) \cong V_Q \tag{13}$$

This indicates from eqs 1 and 2 that

$$\Delta G^*(\text{Z}) = \Delta G^*(\text{X}) - mkT\ln\frac{V(\text{max})}{V(\text{min})} < \Delta G^*(\text{X})$$

$$B(\text{Z}) = B(\text{X}) - m\Delta T\ln\frac{V(\text{max})}{V(\text{min})} < B(\text{X})$$

or

$$\sigma_e\sigma\,(\text{Z}) < \sigma_e\sigma\,(\text{X}) \tag{14}$$

where (Z) and (X) indicate physical quantities around the Z- and X-axes, respectively. Here we assumed that $V_0(Z) \cong V_0(X)$ and that T_m^0 under shear flow was the same as that in quiescent state.[16] Equation 14 indicates that $\sigma_e\sigma$ (X) correspond to $\sigma_e\sigma$ within the usual isotropic melt ($\sigma_e\sigma_{(\text{iso})}$). As $\sigma_e\sigma(Z) < \sigma_e\sigma_{(\text{iso})}$, the $\sigma_e\sigma(Z)$ should correspond to $\sigma_e\sigma$ within the "oriented melt" ($\sigma_e\sigma_{(\text{ori})}$). Thus, it is concluded that the oriented and isotropic melt are formed around the Z- and X-axes on the interface of a spiralite, respectively. Hence we have

$$V(\text{max}) = V_{\text{ori}}$$

and

$$V(\text{min}) = V_{\text{iso}} \tag{15}$$

where V_{ori} and V_{iso} are growth rates in the oriented and isotropic melt, respectively.

Therefore, it is concluded that appearance of V(max) and V(min) are evidences of formation the oriented and isotropic melt around the Z- and X-axes, respectively. Growth rate was accelerated around interface even when macro $\dot{\gamma}$ is low.

3.7. Angular Velocity of the "Spiralite". Φ was plotted against t in Figure 9. Φ increased linearly with increase of t

$$\Phi = \Omega\, t + C \tag{16}$$

where Ω is angular velocity and C is a constant. Thus, Ω and C were obtained

$$\Omega \equiv \frac{d\Phi}{dt} = 1.8 \times 10^{-2}\text{rad/s} \quad \text{and} \quad C = -7.9\ (\text{rad}) \tag{17}$$

Therefore, we have

$$\Omega = \frac{1}{6}\dot{\gamma} \ll \dot{\gamma} = 0.1\ \mathrm{s}^{-1} \tag{18}$$

$\Omega \ll \dot{\gamma}$ is natural in the case of viscous fluid. It is concluded that Ω is much smaller than $\dot{\gamma}$ at around the *Z*-axis. We will show in section 4.1 that this takes an important role in the formation of the oriented melt.

3.8. Archimedes Spiral. r_{OA} is the radius of a point A on the solid curved line and θ is angle of the r_{OA} measured from the origin (Figure 6a). The direction of r_{OA} at the origin ($\theta \cong 0$) is described by a line OB.

r_{OA} was plotted against θ (Figure 10). r_{OA} increased linearly with increasing of θ and became constant (denoted by r) at a breaking point(θ_b) at $\theta_b \cong 3\pi$, that is

$$\begin{aligned} r_{OA} &= a\theta \quad \text{for } \theta \le \theta_b \cong 3\pi \\ &= \text{const} \equiv r \quad \text{for } \theta > \theta_b \end{aligned} \tag{19}$$

where $a = 10\ \mu$m/rad. Therefore, it is concluded that the spiral pattern is Archmedes spiral for $\theta \le \theta_b$. Therefore, outline of the spiralite shown by the dashed curve is a circle. As r increased with increase of t, r is written by $r(t)$.

4. Theory: Mechanism of Acceleration of Growth Rate Under Shear Flow

4.1. Increase of Strain Rate $\dot{\gamma}$ on the Interface. We will show why $\dot{\gamma}$ becomes locally very high on the interface under shear flow. Figure 11 shows a schematic illustration of the cross section of a crystal within the melt under shear flow. To simplify, we assume a circular shape. It is to be noted that the following discussion is not limited to the circular shape but also may be applied to any shape of crystal, such as spherulite, shish, solid particle, or dust and so on.

We will discuss "micro velocity and micro shear rate (v(Z) and $\dot{\gamma}$(Z))" around interface within the melt as a function of *Z*. $\dot{\gamma}$(Z) is defined by

$$\dot{\gamma}(\mathrm{Z}) \equiv \frac{\mathrm{d}v(\mathrm{Z})}{\mathrm{dZ}} \tag{20}$$

If the crystal is omitted, the melt corresponds to usual shear flow melt. Therefore, the v(Z) denoted by $v_{\dot{\gamma}}$(Z) is given by

$$v(\mathrm{Z}) = \dot{\gamma}\mathrm{Z} \equiv v_{\dot{\gamma}}(\mathrm{Z}) \tag{21}$$

v(Z) is illustrated by a straight line.

When a crystal is put in the shear flow melt, the v(Z) should be disturbed by the crystal. The crystal should start rotating with Ω. The velocity along *X*-axis at a point P on the surface of the crystal (v_P) is given by

$$v_P = \Omega\, r_{OP} \tag{22}$$

where r_{OP} is the radius between O and P. As the melt cannot slip at P on the surface of the crystal that is well-known

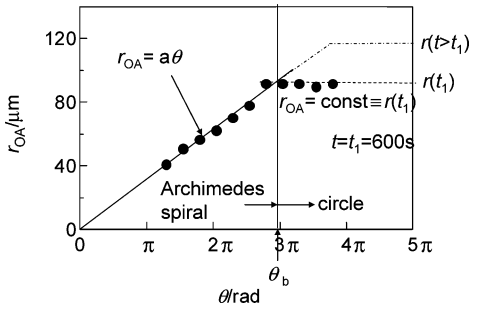

Figure 10. Plots of r_{OA} of a spiral pattern of PB-1 against θ ($\dot{\gamma} = 0.1\ \mathrm{s}^{-1}$, $T_c = 102$ °C). r_{OA} increased linearly with increase of θ up to θ_b and was constant for $\theta > \theta_b$.

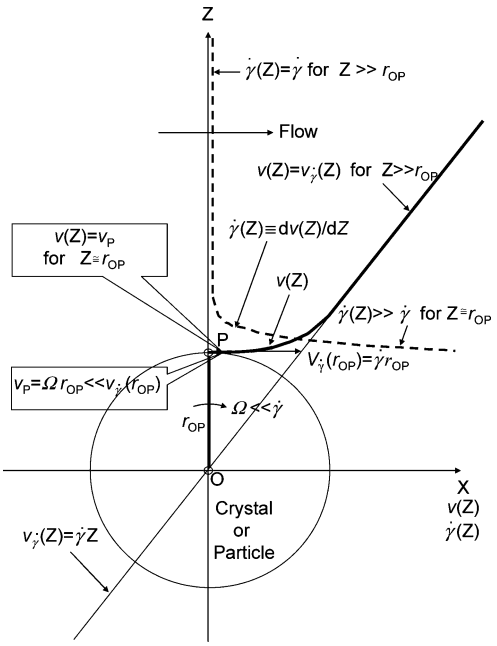

Figure 11. Schematic illustration of mechanism of increase of micro $\dot{\gamma}$(Z) on the interface of crystal or particle under shear flow. v(Z) (heavy curve) continuously increases from v_P and approaches to $v_{\dot{\gamma}}$(Z) with increase of *Z*. $\dot{\gamma}$(Z) (broken curve) significantly increases near the interface. The essential reason for significant increase of $\dot{\gamma}$(Z) is due to $\Omega \ll \dot{\gamma}$.

boundary condition, the velocity of the melt at P should be equal to v_P, i.e.

$$v(\mathrm{Z}) = v_P \quad \text{for } \mathrm{Z} \cong r_{OP} \tag{23}$$

From eqs 18, 22, and 23, we have

$$v(\mathrm{Z}) \ll v_{\dot{\gamma}}(\mathrm{Z}) \quad \text{for } \mathrm{Z} \cong r_{OP} \tag{24}$$

It is obvious that v(Z) approaches $v_{\dot{\gamma}}$(Z) for $Z \gg r_{OP}$, i.e.

$$v(\mathrm{Z}) = \dot{\gamma}\mathrm{Z} \equiv v_{\dot{\gamma}}(\mathrm{Z}) \quad \text{for } \mathrm{Z} \gg r_{OP} \tag{25}$$

because the crystal does not disturb the flow at all. Thus, the v(Z) continuously increases from v_P and approaches to $v_{\dot{\gamma}}$(Z) with increase of *Z* shown by a heavy curve.

Finally we have

$$\begin{aligned} \dot{\gamma}(\mathrm{Z}) &\gg \dot{\gamma} \quad \text{for } \mathrm{Z} \cong r_{OP} \\ &\cong \dot{\gamma} \quad \text{for } \mathrm{Z} \gg r_{OP} \end{aligned} \tag{26}$$

The $\dot{\gamma}$(Z) is illustrated by a broken curve in Figure 11.

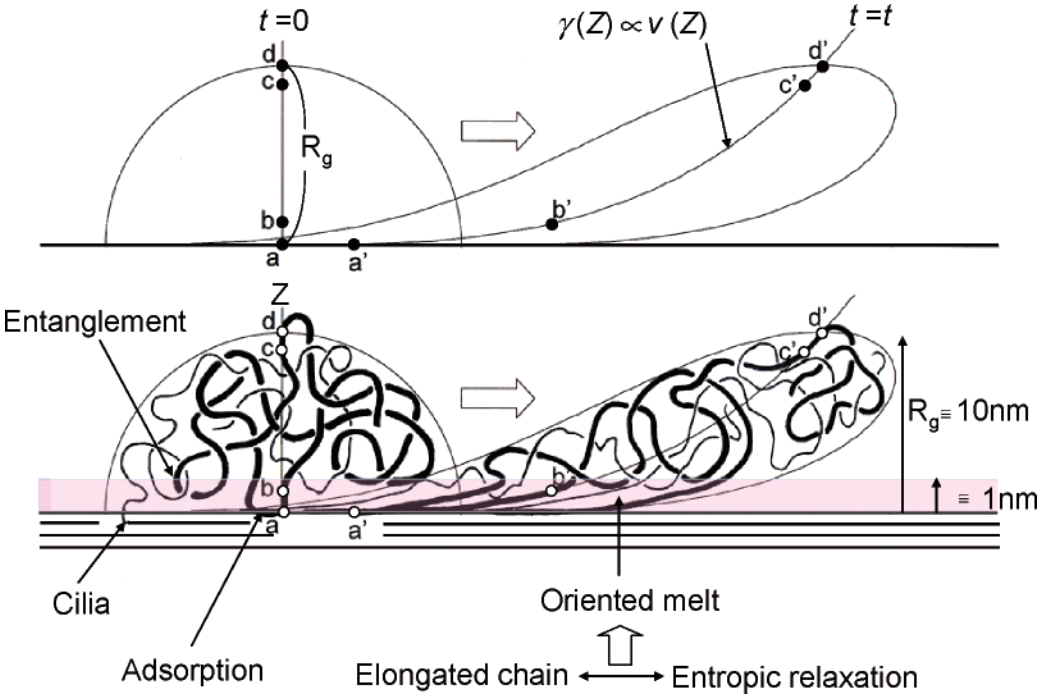

Figure 12. Schematic illustrations of mechanism of the oriented melt near the interface of a crystal under shear flow. When the macro $\dot{\gamma}$ increases significantly, the effect of the elongation will overcome that of the entropic relaxation, that results in the formation of the steady "oriented melt". (a) Change from random coil to "tear shape". (b) Change of conformation of molecular chains. As a lot of entanglements, adsorbed segments and some "cilias" exist near the interface and they results in "topological restriction" to the entropic relaxation, they should significantly suppress the entropic relaxation and the oriented melt is easily formed.

Thus, we have a conclusion that the $\dot{\gamma}(Z)$ significantly increases near the interface of the crystal even when macro $\dot{\gamma}$ is low. An essential reason for a significant increase of micro $\dot{\gamma}(Z)$ is due to $\Omega \ll \dot{\gamma}$ (eq 18). As $\Omega \ll \dot{\gamma}$ can be generally expected for viscous fluid, "the increase of micro $\dot{\gamma}(Z)$" should be universally expected on the interface of any solid particle within the melt.

4.2. Mechanism of Formation of the Oriented Melt. We will propose in this section a mechanism of formation of the locally oriented melt of polymer around interface under shear flow. When we start adding shear to the sample at $t = 0$, $\dot{\gamma}(Z)$ and $v(Z)$ should be seen on the interface of a crystal (Figure 12). The conformation of an adsorbed random coil[17] will be elongated after $t = t$ due to $v(Z) = \dot{\gamma}(Z)Zt$. Actually elongated chains will be relaxed due to entropic agitation. This means that the elongation and entropic relaxation of chains compete with each other. As a result the strain $\gamma\ (Z) \propto v(Z) = \dot{\gamma}(Z)Zt$ should be expected (Figure 12a). As $\dot{\gamma}(Z)$ significantly increases near the surface, the relative chain distance "*ab*" near the surface($\cong$ 1 nm) is significantly elongated to "$a'b'$ ", while the distance "*cd*" far from the surface ($R_g \cong 10$ nm) changes only a little to "$c'd'$ ". Thus, the chain conformation changes from random coil to "tear shape".

When the macro $\dot{\gamma}$ increases significantly, the effect of the elongation will overcome that of the entropic relaxation, that results in the formation of the steady "oriented melt". We can predict that a critical $\dot{\gamma}$ ($=\dot{\gamma}^*$) exists for formation of the oriented melt. As a lot of entanglements, adsorbed segments, and some "cilias" exist near the interface (Figure 12b) and they result in "topological restriction" to the entropic relaxation, they should significantly suppress the entropic relaxation, and the oriented melt is easily formed. Thus, we can predict that the formation of the oriented melt becomes much easier with increases of the topological restriction, which can be expected for increases of M_w, entanglement, and so on.

4.3. Possible Relationship between Melt Structure and Crystallization. We will propose a possible relationship between melt structure and crystallization (Table 1) coupled with the previous works[1−12] and this work that is marked by an asterisk (∗). This is important and useful for understanding the relative relationship and for polymer processing. In the case of the polymer system, there are three kind of external fields, i.e., elogational, shear, and quiescent ones. The former two and the last are anisotropic fields and an isotropic field, respectively.

In the case of elongational field with $\dot{\epsilon}$ higher than a critical one ($\dot{\epsilon}^*$), chains are easily elongated and the uniform oriented melt should be formed, as has been shown by Kotaka et al.[1,2] This results in acceleration of I_{ori} and V_{ori} and novel morphologies of row-nucleation, shish, kebab, or transcrystal, where I_{ori} is nucleation rate within the oriented melt.

Shear field is classified into high ($\dot{\gamma} > 10^2 s^{-1}$) and low ($\dot{\gamma} < 10\ s^{-1}$) ones. In the case of high uniform macro shear field, with $\dot{\gamma}$ higher than a critical one ($\dot{\gamma}^*$), chains are elongated and the "uniform oriented melt" should be formed within the bulky melt, that results in acceleration of I_{ori} and V_{ori}, as Fritzsche et al.[3] showed, and row-nucleation, shish, kebab, or transcrystal should be formed.

In the case of a low uniform macro shear field within the bulky melt, chains are relaxed due to entropic relaxation and the isotropic melt should be formed, which results in small I_{iso} and V_{iso} spherulite, axiallite, etc. will be formed, where I_{iso} is the nucleation rate within the isotropic melt.

Even in the case of low macro $\dot{\gamma}$, this study showed that nonuniform micro shear field should be expected around interface of any crystal within the melt, and chains should be elongated and the locally oriented melt should be formed, as is shown in Figure 13 that results in acceleration of V_{ori}. The same mechanism should be expected on the interface of any solid material, such as dust or nucleating agents, as is shown in Figure 13. In this case, the locally oriented melt should be formed,

Table 1. Possible Relationship between Melt Structure and Crystalization[a]

External field				Dominant mechanism	Melt structure		Crystallization	
							I, *V*	Morphology
Anistropic	Shear*, Elongation	High ($\dot{\gamma}$or $\dot{\varepsilon}$>>10s^{-1})	Uniform macro $\dot{\gamma}$ within bulky melt	Chain elongation*	Oriented melt*	Uniform	Large V^*_{ori}, I_{ori} (acceleration)	Row-nucleation, Shish, Kebab, Transcrystal / Skin
		Non-* uniform micro $\dot{\gamma}$ around interface of solid				Local*		Spiralite*
		Low*($\dot{\gamma}$ or $\dot{\varepsilon}$<10s^{-1})	Uniform* macro $\dot{\gamma}$ within bulky melt	Entropy* relaxation	Isotropic melt*		Small V^*_{iso}, I_{iso}	Spherulite*, Axiallite etc. / Core
Isotropic	Quiescent*							

[a] The asterisk denotes items dealt with in this work.

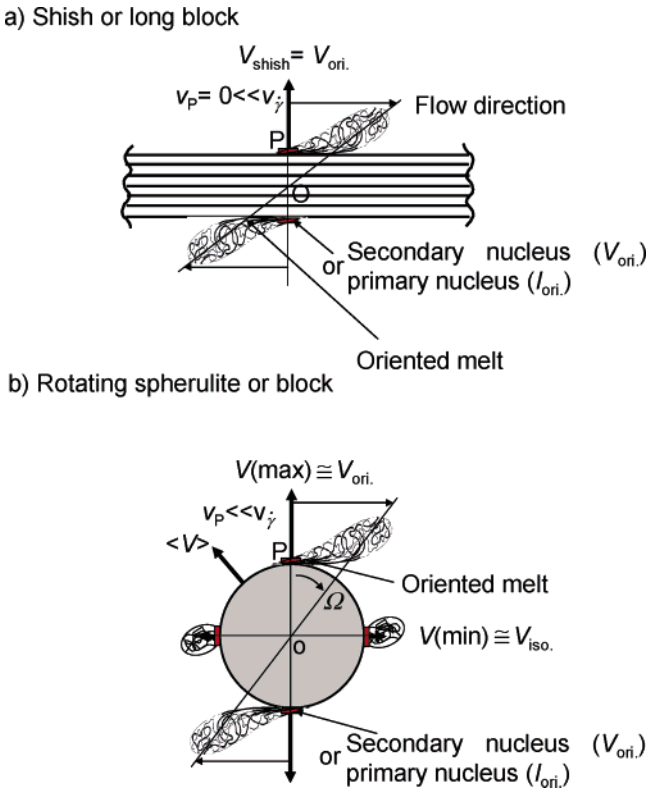

Figure 13. Schematic illustrations of mechanism of acceleration of growth and nucleation rates around interface of the (a) shish or long block and (b) rotating spherulite or block under low shear rate flow.

that results in acceleration of heterogeneous primary nucleation rate (I_{ori}). Parts a and b of Figure 13 illustrate acceleration mechanism of V_{ori} or I_{ori} on the interface of long crystals (such as shish) or solid materials whose length is too long to rotate and rotating crystals (such as spherulites) or solid materials, respectively. Acceleration of V_{ori} of shish was experimentally shown by us in Figures 6A and 7A in ref 8. Thus, V_{ori} and I_{ori} should be accelerated, and row-nucleation, shish, kebab, or transcryatal will be formed.

In the case of quiescent field, chains are fully relaxed due to entropic relaxation and the isotropic melt should be formed, that results in small I_{iso} and V_{iso} and spherulite or axiallite etc. will be formed.

In injection type processing, $\dot{\gamma}$ significantly increases near the mold wall surface and row-nucleation, shish, kebab, or transcrystal forms the "skin layers", while $\dot{\gamma}$ is small at the center in the mold and spherulite and axiallite etc. form the "core layers".

5. Conclusion

(1) We found a novel morphology of "spiral pattern" on the top surface of a rotating "half-spherulite" under low shear rate flow, when the spherulite nucleates near the free surface of the melt. We named the half-spherulite "spiralite".

(2) The "spiralite" rotates showing large and small growth rates (V(max) and V(min)) along directions perpendicular and parallel to the flow direction (Z- and X-axes), respectively. The anisotropic growth rates $V(\text{max}) = V(Z)$ and $V(\text{min}) = V(X)$ were directly obtained by using the rotation of the "spiral pattern".

(3) We proved the formation of the "oriented melt" on the interface around the Z-axis of a spiralite from the observed anisotropic $V(Z)$ and $V(X)$.

(4) We explained theoretically the formation mechanism of the oriented melt: as "micro shear rate $\dot{\gamma}(Z)$" on the interface around the Z-axis significantly increases, chains will be elongated even when "macro $\dot{\gamma}$" is low. With increase of $\dot{\gamma}(Z)$, the chain elongation will overcome the entropic relaxation, that results in formation of the "oriented melt".

(5) We proposed acceleration mechanism of growth and nucleation rates under shear flow due to formation of the oriented melt. We proposed a possible relationship between the melt structure and crystallization under anisotropic and isotropic external fields.

Acknowledgment. We thank Dr. T. Takahashi, Y. Tsuzuki in Yamagata University and Dr. K. Tagashira in SunAllomer Ltd. for their helps and supports in experiments.

References and Notes

(1) Kotaka, T.; Kojima, A.; Okamoto, M. *Rheol. Acta* **1997**, *36*, 646.
(2) Okamoto, M.; A, Kojima.; Kotaka, T. *Polymer* **1998**, *39*, 2149.

(3) Fritzsche, A. K.; Price, F. P. *Polym. Eng. Sci.* **1974**, *14*, 401.
(4) Monasse, B. *J. Mater. Sci.* **1995**, *30*, 5002.
(5) Wolkowicz, M. D. *J. Polym. Sci. Polym. Symp.* **1978**, *63*, 365.
(6) Ulrich, R. D.; Price, F. P. *J. Appl.Polym.Sci.***1976**, *20*, 1077.
(7) Yamazaki, S.; Watanabe, K.; Okada, K.; Yamada, K.; Tagashira, K.; Toda, A.; Hikosaka, M. *Polymer, Part 1* **2005**, *46*, 1675.
(8) Yamazaki, S.; Watanabe, K.; Okada, K.; Yamada, K.; Tagashira, K.; Toda, A.; Hikosaka, M. *Polymer, Part 2* **2005**, *46*, 1685.
(9) Lieberwirth, I.; Loos, J.; Petermann, J.; Keller, A. *J. Polym. Sci. Part B Polym. Phys.* **2000**, *38*, 1183.
(10) Hosier, I. L; Bassett, D. C. *Polymer* **1995**, *36*, 4197.
(11) Alfonso, G. C.; Azzurri, F. *Flow induced crystallization of polymers Impact to processing and manufact properties*; 2001; p 27.
(12) Monasse, B. *J. Mater. Sci.* **1992**, *27*, 6047.
(13) Turnbull, D.; Fishear, J. C. *J.Chem. Phys.* **1949**, *17*, 71.
(14) López, L. C.; Cieslinski, R. C.; Putzig, C. L.; Wesson, R. D. *Polymer* **1995**, *36*, 2331.
(15) Watanabe, K.; Nagatake, W.; Takahashi, T.; Masubuchi, Y.; Takimoto, J.; Koyama, K. *Polym. Test.* **2003**, *22*, 101.
(16) Yamazaki, S.; Hikosaka, M.; Toda, A.; Wataoka, I.; Yamada, K.; Tagashira, K. *J. Macromol. Sci., Part B: Phys.* **2003**, *B42*, 499.
(17) Takahashi, A. *J. Surf. Sci. Soc. Jpn. Hyomen Kagaku* **1989**, *10* (10), 142.

MA050825Z